Constraints on the Redshift Evolution of the L_X-SFR Relation from the Cosmic X-Ray Backgrounds

Mark Dijkstra[1]⋆, Marat Gilfanov[1,2], Abraham Loeb[3], and Rashid Sunyaev[1,2]

[1] *Max-Planck Institut fuer Astrophysik, Karl-Schwarzschild-Str. 1, 85741 Garching, Germany*
[2] *Space Research Institute of Russian Academy of Sciences, Profsoyuznaya 84/32, 117997 Moscow, Russia*
[3] *Astronomy Department, Harvard University, 60 Garden Street, Cambridge, MA 02138, USA*

1 December 2011

ABSTRACT
Observations of local star forming galaxies have revealed a correlation between the rate at which galaxies form stars and their X-Ray luminosity. We combine this correlation with the most recent observational constraints on the integrated star formation rate density, and find that star forming galaxies account for 5-20% of the total soft and hard X-ray backgrounds, where the precise number depends on the energy band and the assumed average X-ray spectral energy distribution of the galaxies below ~ 20 keV. If we combine the L_X-SFR relation with recently derived star formation rate function, then we find that star forming galaxies whose X-ray flux falls well (more than a factor of 10) below the detection thresholds of the Chandra Deep Fields, can fully account for the unresolved soft X-ray background, which corresponds to $\sim 6\%$ of its total. Motivated by this result, we put limits on the allowed redshift evolution of the parameter $c_X \equiv L_X/\mathrm{SFR}$, and/or its evolution towards lower and higher star formation rates. If we parametrize the redshift evolution of $c_X \propto (1+z)^b$, then we find that $b \leqslant 1.3$ (95% CL). On the other hand, the observed X-ray luminosity functions (XLFs) of star forming galaxies indicate that c_X may be increasing towards higher redshifts and/or higher star formation rates at levels that are consistent with the X-ray background, but possibly at odds with the locally observed L_X-SFR relation.

Key words: galaxies: high redshift – galaxies: stellar content – X-rays: binaries – X-rays: galaxies

1 INTRODUCTION

Galaxies contain various sources of X-ray emission which include: (*i*) active galactic nuclei (AGN), which are powered by accretion of gas onto a supermassive black hole (*ii*) hot ($T \gtrsim 10^6$ K) interstellar gas, and (*iii*) X-ray binaries, which consist of a compact object, either a neutron star or a stellar mass black hole, and a companion star from which the compact object accretes mass. The X-Ray luminosity of star forming galaxies without AGN is dominated by so-called high-mass X-ray binaries (HMXBs, e.g. Grimm et al. 2003), in which the neutron star or stellar mass black hole is accreting gas from a companion that is more massive than $\sim 5 M_\odot$. HMXBs are thus tightly linked to massive stars, and since massive stars are short lived, the combined X-ray luminosity of HMXBs is expected to be linked to the rate at which stars form (e.g. Helfand & Moran 2001). The X-Ray luminosity of star forming galaxies is indeed observed to be correlated with the rate at which they are forming stars (Grimm et al.

2003; Ranalli et al. 2003; Gilfanov et al. 2004; Persic et al. 2004; Mineo et al. 2011a; Lehmer et al. 2010; Mineo et al. 2011b; Symeonidis et al. 2011).

This 'L_X-SFR relation' encodes a wealth of information on various astrophysical processes. These include the initial mass function (IMF) of stars, the fraction of massive stars that form in binaries, the mass ratio distribution of binary stars, the distribution of their separations, the gas metallicity, and the common envelope efficiency (e.g. Belczynski et al. 2002; Mineo et al. 2011b, and references therein). Despite its dependence on many astrophysical processes, the L_X-SFR relation is observed to hold over ~ 4 orders of magnitude (Mineo et al. 2011b), with a modest scatter ($\sigma = 0.4$ dex).

Existing observations have only been able to probe the L_X-SFR relation in nearby galaxies. There are observational hints–as well as theoretical expectations– that c_X is higher in low mass galaxies and/or low metallicity environments (Dray 2006; Linden et al. 2010; Kaaret et al. 2011), which suggests that $c_X \equiv L_X/\mathrm{SFR}$ could have been substantially higher at higher redshifts (see Mirabel et al. 2011, for a

---

⋆ E-mail:dijkstra@mpa-garching.mpg.de

summary). However, quantitative constraints on ratio c_X at higher redshifts are virtually non-existent. The main reason is that the X-ray flux that reaches Earth from individual star forming galaxies typically falls well below the detection threshold of existing X-ray telescopes (see § 2).

The relation between SFR and L_X also plays an important role in determining the thermal history of intergalactic medium at very high redshifts (e.g. Oh 2001; Venkatesan et al. 2001), and strongly affects the 21-cm signal from atomic hydrogen during the dark ages (Furlanetto et al. 2006; Pritchard & Furlanetto 2007; Pritchard & Loeb 2010; Alvarez et al. 2010). Current theoretical models of this reheating process explore values for c_X that span ~ 4 orders of magnitude.

The goal of this paper is to investigate whether it is possible to put any constraints on the evolution of c_x with either redshift and/or towards high/low star formation rates than probed by existing observations of individual galaxies, using the cosmic X-Ray backgrounds (CXBs).

Our paper is organized as follows. In § 2, we summarize recent observational constraints on the levels of the total X-ray background (XRB, both soft and hard), as well as the fraction of the XRB that has been resolved in discrete X-ray sources. In § 3 we compute the total contribution of star forming galaxies to the soft and hard X-Ray backgrounds, and show that this contribution can be substantial. In § 4 we show that star forming galaxies, too faint to be detected as individual X-ray sources, can fully account for the unresolved portion of the XRB. In § 5 we put constraints on possible trends in the L_X-SFR relation using the unresolved soft XRB. There are several additional candidate sources which contribute to the unresolved CXBs (these include for example low mass X-ray binaries and weak AGN, see § 6). To constrain the evolution of c_X we will allow the entire unresolved SXB to be produced by HMXBs (and the hot ISM) in X-ray faint star-forming galaxies. This results in conservative upper limits on possible evolution in c_X. Finally, we conclude in § 6. The cosmological parameters used throughout our discussion are $(\Omega_m, \Omega_\Lambda, \Omega_b, h) = (0.27, 0.73, 0.046, 0.70)$ (Komatsu et al. 2009).

2   THE COSMIC X-RAY BACKGROUNDS (CXB)

2.1   The Observed Soft X-ray Background (SXB)

The total soft (E=1-2 keV) CXB (SXB) amounts to $S_{1-2} = 4.6 \pm 0.3 \times 10^{-12}$ erg s^{-1} cm^{-2} deg^{-2} (e.g. Hickox & Markevitch 2006). Hickox & Markevitch (2006) find an unresolved SXB intensity of $1.04 \pm 0.14 \times 10^{-12}$ erg s^{-1} cm^{-2} deg^{-2}, after removing all point and extended sources detected in the *Chandra Deep Fields* (CDFs). The detection threshold in the *Chandra Deep Field-North* (CDF-North) corresponds to $s_{th} \sim 2.4 \times 10^{-17}$ erg s^{-1} cm^{-2} (Alexander et al. 2003; Hickox & Markevitch 2007a).

Hickox & Markevitch (2007a) showed through a stacking analysis that $\sim 70\%$ of the unresolved component is accounted for by sources that are detected with the *Hubble Space Telescope*, but not individually as X-ray sources. Their stacking analysis shows that these X-ray undetected sources have an *average* X-ray flux that is $\langle s \rangle \sim 0.15 - 0.30 s_{th} \sim$

$3.6 - 7.2 \times 10^{-18}$ erg s^{-1} cm^{-2}. Hickox & Markevitch (2007b) find that the cumulative number of these X-ray undetected HST sources brighter than some of X-ray flux s, is well-described by a power-law $N(> s) \propto s^{-\beta}$, where $\beta = 1.1^{+0.5}_{-0.3}$. We can then estimate the minimum X-ray flux, s_{min}, that the HST-detected sources probed from $\langle s \rangle = \int_{s_{min}}^{s_{th}} dS \frac{dN}{dS} S / \left[\int_{s_{min}}^{s_{th}} dS \frac{dN}{dS} \right]$, and find that $s_{min} = 1.2 - 3.2 \times 10^{-18}$ erg s^{-1} cm^{-2} (for $\beta = 1.1$). Throughout, we use the remaining 30% of the unresolved SXB as a measure of the 'true unresolved SXB', which amounts to $3.4 \pm 1.4 \times 10^{-13}$ erg s^{-1} cm^{-2} deg^{-2} (Hickox & Markevitch 2007a), down to a minimum flux s_{min}.

2.2   The Observed Hard X-ray Background (HXB)

The total hard (E=2-8 keV) CXB (HXB) amounts to $S_{2-8} = 1.7 \pm 0.2 \times 10^{-11}$ erg s^{-1} cm^{-2} deg^{-2} (e.g. Hickox & Markevitch 2006). Hickox & Markevitch (2006) find an unresolved HXB intensity of $3.4 \pm 1.7 \times 10^{-12}$ erg s^{-1} cm^{-2} deg^{-2}. We will not use the unresolved HXB to put constraints on the redshift evolution of c_X for two reasons: (i) the uncertainties on the unresolved HXB are larger than for the SXB, and (ii) as we will explain below (§ 3.2) we are much more sensitive to the assumed X-Ray spectrum outside the Chandra bands, when we compare our models to the HXB.

3   THE CONTRIBUTION OF STAR FORMING GALAXIES TO THE CXB

3.1   The Model

The total contribution S_{tot} (in erg s^{-1} cm^{-2} deg^{-2}) of star forming galaxies to the SXB is given by (Appendix B)

$$S_{tot} = \frac{\Delta\Omega}{4\pi} \frac{c}{H_0} \int_0^{z_{max}} \frac{dz}{(1+z)^2 \mathcal{E}(z)} \dot\rho_*(z) \mathcal{L}_X(z, \Gamma). \qquad (1)$$

Here $\Delta\Omega \sim 3.0 \times 10^{-4}$ sr deg^{-2}, $\mathcal{E}(z) = \sqrt{\Omega_m(1+z)^3 + \Omega_\Lambda}$, and $\dot\rho_*(z)$ denotes the comoving star formation rate density at redshift z (in $M_\odot$ yr^{-1} cMpc^{-3}, where 'cMpc' stands for co-moving Mpc). We adopt the star formation history from Hopkins & Beacom (2006), using the parametric form $\dot\rho_*(z) = (a + bz)h/(1 + (z/c)^d)$ from Cole et al. (2001), where $a = 0.017$, $b = 0.13$, $c = 3.3$, and $d = 5.3$. We note that the amplitude of the function $\dot\rho_*(z)$ depends on the assumed IMF (see Hopkins & Beacom 2006, for a more detailed discussion). The adopted normalization derives from classical Salpeter IMF (Salpeter 1955) between 0.1 to $100 M_\odot$ (Hopkins 2004). The same IMF was assumed in the derivation of the SFR-L_X relation (see Mineo et al. 2011b), and our calculations are therefore self-consistent.

The term $\mathcal{L}_X(z, \Gamma) \equiv c_X K(z, \Gamma)$ denotes the 'K-corrected' X-ray luminosity (in erg s^{-1}) per unit star formation rate in the *observed* energy range E$_1$-E$_2$. In this paper, E$_1 = 1.0$ keV and E$_2 = 2.0$ keV for the soft band, and E$_1 = 2.0$ keV and E$_2 = 8.0$ keV for the hard band. Mineo et al. (2011b) recently determined[1] the value of $c_X \equiv L_X/$SFR,

---

[1] The literature contains values for c_X that at face value ap-
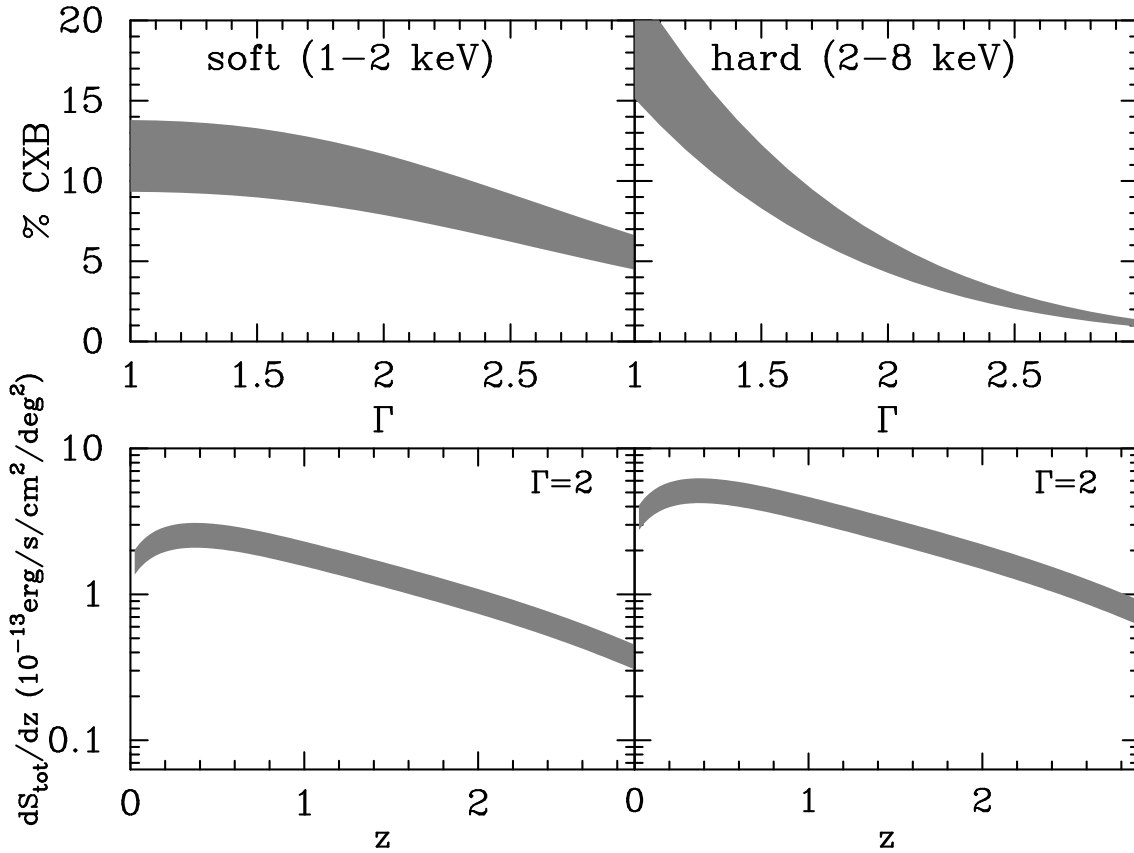
Figure 1. The *top panels* show the fraction of the total soft (*left*) and hard (*right*) X-Ray backgrounds that can be attributed to star forming galaxies, as a function of the assumed photon index Γ, for power-law X-Ray spectral energy distributions (see text). We have drawn curves for a range of observed values for $c_{\rm X} \equiv L_{\rm X}/{\rm SFR}$ (see text). Depending on the assumed value for Γ, star forming galaxies can account for $\sim 5-15\%$ of the total observed soft X-ray background, and up to $\sim 20\%$ of the hard X-ray background. For comparison, Swartz et al. (2004) found that typically ULX spectra in the Chandra bands could be described by a powerlaw with $\langle\Gamma\rangle = 1.7$, which would place the contribution of star forming galaxies to the soft X-ray background at $\sim 9-13\%$. As the spectra of ULXs at $E > 10$ keV are poorly known, the contribution of star forming galaxies to the hard X-ray background is more uncertain. The *lower panels* show that the contribution per unit redshift, $dS_{\rm tot}/dz$, peaks at low redshift $z \sim 0.4-0.5$.

where SFR denotes the star formation rate in $M_\odot$ yr^{-1}, to be $c_{\rm X} = 2.6\times10^{39}$ erg s$^{-1}/[M_\odot$ yr$^{-1}]$ when only compact resolved X-Ray sources in galaxies are included. Mineo et al. (2011b) also found that the best fit $c_{\rm X,max} = 3.7 \times 10^{39}$ erg s^{-1} $[M_\odot$ yr$^{-1}]^{-1}$ for unresolved galaxies in the *Chandra Deep Field North* and ULIRGs. However, a non-negligible fraction of this additional unresolved flux is in a soft component, and would not contribute to soft X-Ray background (measured in the 1-2 keV band, see Bogdan & Gilfanov 2011). We will not attempt to model in detail the contribution of unresolved X-Ray emission. Instead, Figures 1, 2, and

pear both lower (e.g. Persic & Rephaeli 2007) and higher (e.g. Ranalli et al. 2003) by a factor of a few. However, some studies measured the X-Ray luminosity ($L_{\rm X}$) in the range 2-10 keV (e.g. Gilfanov et al. 2004; Persic et al. 2004; Persic & Rephaeli 2007; Lehmer et al. 2010), or 0.5-2.0 keV (Ranalli et al. 2003). Furthermore, some studies have derived values for $c_{\rm X}$ using a formation rate of stars (SFR) in the mass range $5 \leqslant M/M_\odot \leqslant 100$ (e.g. Persic et al. 2004), which results in larger values for $c_{\rm X}$. Mineo et al. (2011b) discuss that most studies are consistent with their derived value when identical definitions for 'SFR' and '$L_{\rm X}$' are used.

4 show our results for the full range $c_{\rm x} = 2.6-3.7\times10^{39}$ erg s^{-1} $[M_\odot$ yr$^{-1}]^{-1}$. We point out that Mineo et al. (2011b) measured the X-ray luminosity over the energy range $0.5-8$ keV.

This observed relation between $L_{\rm X}$ and SFR holds over ~ 4 orders of magnitude in SFR from SFR$\sim 0.1-1000$ $M_\odot$ yr^{-1}, with a scatter of $\sigma \sim 0.4$ dex. We include this scatter in our calculation by convolving equation (1) with a lognormal probability distribution function for $c_{\rm X}$ with a mean of $\langle\log c_{\rm X}\rangle = 39.4$ and standard deviation of $\sigma = 0.4$ (see Fig. 9 of Mineo et al. 2011b). Because the log-normal distribution is symmetric in $\log c_{\rm X}$, it is skewed towards larger values of $c_{\rm X}$ in linear coordinates. The observed scatter in the $L_{\rm X}$-SFR relation therefore enhances our computed contributions to the X-ray backgrounds. In the absence of this scatter, $S_{\rm tot}$ reduces by a factor of $\exp\left(-\frac{1}{2}\sigma^2\ln^2 10\right) \sim 0.65$.

Finally, to compute the contribution of a galaxy at redshift z to the CXB in the observed energy range E$_1$-E$_2$, we need to compute the galaxy's luminosity in the range [E$_1$-E$_2$]$\times(1 + z)$ keV. In analogy to the standard 'K-correction' (e.g. Hogg et al. 2002), we multiply $c_{\rm X}$ by $K_{\rm X}(z,\Gamma) = \mathcal{I}(E_1(1 + z), E_2(1 + z))/\mathcal{I}(0.5$ keV$, 8.0$ keV$)$. Here, $\mathcal{I}(x,y) = \int_x^y En(E)dE$, where $n(E)dE$ denotes the

number of emitted of photons in the energy range $E \pm dE/2$. Note that we assume that the X-Ray SED does not depend on the star formation rate ψ. In this paper, we explore power law SEDs for the form $n(E) \propto E^{-\Gamma}$, and the integrals $\mathcal{I}(x, y)$ can be evaluated analytically. Finally, we take the redshift integral from $z_{\min} = 0$ to $z_{\max} = 10$. The results are only weakly dependent on the integration limits we pick, as long as $z_{\max} \geqslant 4.0$ (see the *lower right panel* of Fig. 2).

3.2   Results

The *top panels* of Figure 1 show the fraction of the total soft (*left panel*, 1-2 keV) and hard (*right panel*, 2-8 keV) X-Ray backgrounds that can be attributed to star forming galaxies, as a function of the assumed photon index Γ, and for a realistic range of c_X (see above). Depending on the assumed value for Γ, star forming galaxies can account for $\sim 5-15\%$ of the total soft X-ray background, and up to $\sim 20\%$ of the observed hard X-ray background. For comparison, Swartz et al. (2004) found that the observed distribution of Γ for ultra luminous X-ray sources (ULXs) had a mean $\langle \Gamma \rangle = 1.7$, and mode (i.e. most likely value) of $\Gamma_{\rm pk} \sim 2.0$ in the Chandra bands. For the range $\Gamma = 1.7 - 2.0$ the contribution of star forming galaxies to the soft X-ray background is $\sim 8 - 13\%$. The contribution to the hard XRB depends more strongly on Γ because for this calculation, the K-correction involves a larger extrapolation of the assumed SED, which is poorly known at $E > 10$ keV.

The *lower panels* show the differential contribution as a function of redshift. This differential contribution is given by $dS_{\rm tot}/dz$. These plots show that $dS_{\rm tot}/dz$ peaks at $z \sim 0.38$, and that the dominant contribution to the total X-Ray background comes from lower redshifts. Indeed, $\sim 50\%$ [$\sim 25\%$] of the total contribution comes from $z \lesssim 1.3$ [$z \lesssim 0.8$] (see § 4.2).

4   CONTRIBUTION OF X-RAY FAINT STAR FORMING GALAXIES TO THE SXB

4.1   The Model

We can compute the contribution S_X of star forming galaxies, *fainter than some observed soft X-ray flux $s_{\max}$*, to the SXB as

$$S_X = \frac{\Delta \Omega}{4\pi} \frac{c}{H_0} \int_0^{z_{\max}} \frac{dz}{(1+z)^2 \mathcal{E}(z)} \times \qquad (2)$$

$$\int_0^{L_{\rm X,max}} d\log L_{\rm X} \, n(\log L_{\rm X}, z) \, L_{\rm X} K_{\rm X}(z, \Gamma),$$

where $n(\log L_{\rm X}, z) d\log L_{\rm X}$ denotes the comoving number density of star forming galaxies with X-ray luminosities in the range $\log L_{\rm X} \pm d\log L_{\rm x}/2$ (i.e. the units of $n(\log L_{\rm X}, z)$ are cMpc^{-3} dex^{-1}). Here, $L_{\rm X}$ denotes the X-ray luminosity of galaxies in the 0.5-8.0 keV (restframe). The integral over $L_{\rm X}$ then extends up to $L_{\rm X,max} \equiv 4\pi d_{\rm L}^2(z) s_{\max}/K_{\rm X}(z, \Gamma)$, where $d_{\rm L}(z)$ is the luminosity distance to redshift z. The quantity $n(\log L_{\rm X})$, also referred to as the X-ray luminosity function (XLF) of star forming galaxies, is given by

$$n(\log L_{\rm X}, z) = \int_{\psi_{\min}}^{\psi_{\max}} d\psi \, n(\psi, z) P(\log L_{\rm X}|\psi), \qquad (3)$$

where $n(\psi, z) d\psi$ denotes 'star formation rate function', which gives the comoving number density of galaxies that are forming stars at a rate SFR$= \psi \pm d\psi/2$ at redshift z. The function $P(\log L_{\rm X}|\psi) d\log L_{\rm x}$ denotes the probability that a galaxy that is forming stars at a rate ψ has an X-ray luminosity in the range $\log L_{\rm X} \pm d\log L_{\rm X}/2$. We describe both functions in more details below. We start the integral over ψ at $\psi_{\min} = 10^{-3} M_\odot$ yr^{-1}, which corresponds approximately to the SFR that is theoretically expected to occur in dark matter halos of mass $M_{\rm halo} \sim 10^8 M_\odot$ (Wise & Cen 2009; Trac & Cen 2007; Zheng et al. 2010). Our final results depend only weakly on $\psi_{\min}$ (see the *upper left panel* of Fig. 2). The ψ-integral extends up to $\psi_{\max} = 10^5 M_\odot$ yr^{-1}, with our results being insensitive to this choice.

In the local Universe ($z \sim 0$), the function $n(\psi, z)$ [units are cMpc^{-3} $(M_\odot$ yr$^{-1})^{-1}$] appears[2] to be described accurately by a Schechter function (Bothwell et al. 2011)

$$n(\psi, z) = \frac{\Phi^*}{\psi^*} \left(\frac{\psi}{\psi^*}\right)^\alpha e^{-\psi/\psi^*}, \qquad (4)$$

where $\alpha = -1.51 \pm 0.08$, $\Phi^* = (1.6 \pm 0.4) \times 10^{-4}$ cMpc^{-3}, and $\psi^* = 9.2 \pm 0.3 M_\odot$ yr^{-1}. The redshift evolution of $n(\psi, z)$ is not well known. We assume throughout that $\alpha(z) = -1.51 - 0.23 g(z)$, where $g(x) \equiv \frac{2}{\pi} \arctan x$ is a function that obeys $g(0) = 0$ and $\lim_{z \to \infty} g(z) = 1$. This steepening of the low-end of the star formation rate function at higher redshifts reflects the steepening of UV luminosity functions towards higher redshifts (e.g. Arnouts et al. 2005, Reddy & Steidel 2009, Bouwens et al. 2006, 2007,2008), and the observation that dust-obscuration is negligible for the UV-faint galaxies (e.g. Bouwens et al. 2009). The factor '-0.23' causes $\alpha \to -1.74$ at high redshift, which corresponds to the best-fit slope of the UV-luminosity function of $z = 6$ drop-out galaxies (Bouwens et al. 2007). The redshift evolution of Φ^* and ψ^* is more difficult to infer from the redshift evolution of the UV luminosity functions, because of dust. We have taken two approaches: we constrain either the redshift evolution of Φ^* or ψ^*-while keeping the other fixed- to match the inferred redshift evolution of the star formation rate density (see Appendix A for more details). In reality, we expect both parameters to evolve with redshift, and that our two models bracket the range of plausible more realistic models.

The function $P(\log L_{\rm X}|\psi)$ is given by a lognormal distribution

$$P(\log L_{\rm X}|\psi) = \frac{1}{\sqrt{2\pi}\sigma} \exp\left[\frac{-\left(\log \frac{L_{\rm X}}{\langle L_{\rm X}\rangle}\right)^2}{2\sigma^2}\right], \qquad (5)$$

where $\langle L_{\rm X} \rangle = c_{\rm X} \times \psi$ denotes the X-ray luminosity (measured in the 0.5-8.0 keV rest frame) that is expected from the observed SFR-$L_{\rm X}$ relation. The standard deviation $\sigma = 0.4$ denotes the observed scatter in this relation (Lehmer et al. 2010; Mineo et al. 2011b). Ranalli et al. (2005) made very similar predictions for the XLFs, but instead of using star formation rate functions, they used galaxy luminosity functions in various bands. Ranalli et al. (2005) also

---

[2] Previous work showed that this star formation rate function can be described by a log-normal function (Martin et al. 2005). However, this lognormal function does not provide a good fit to the observed star formation rate function particularly for low and high star formation rates (see Fig 4 of Bothwell et al. 2011).
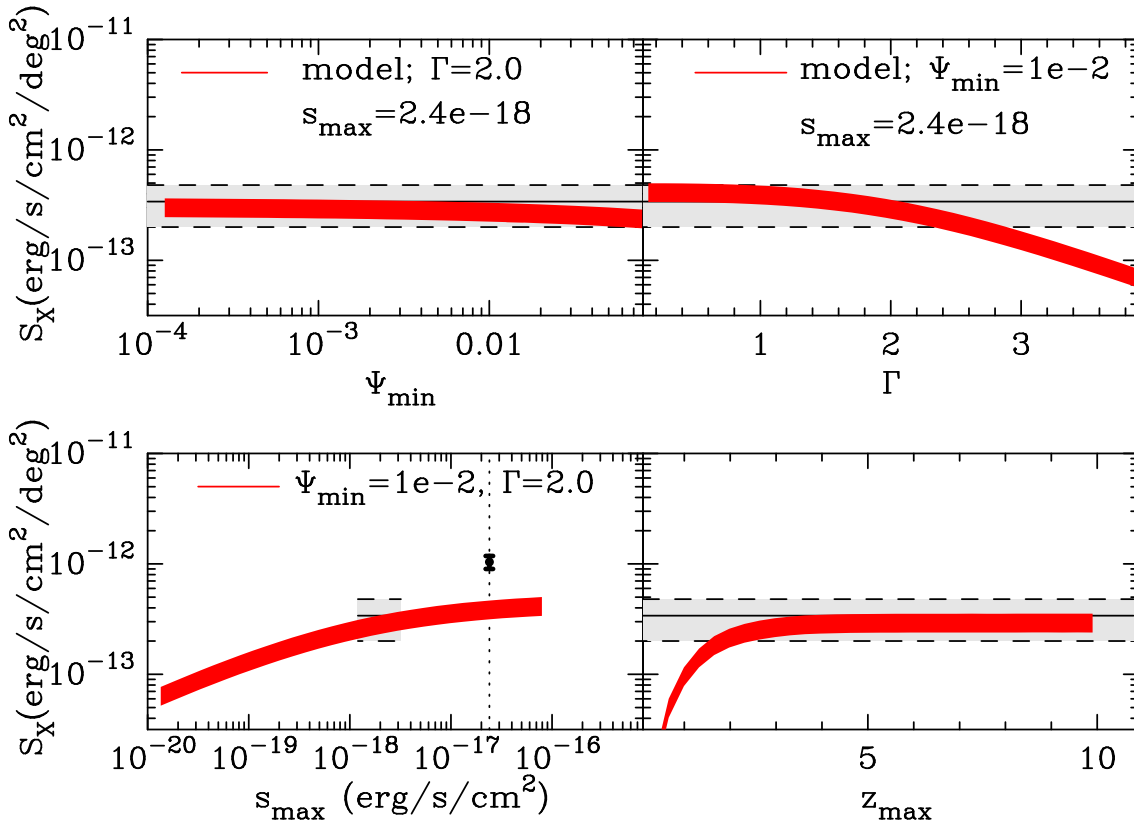
Figure 2. The contribution S_X to the soft X-Ray background (SXB, E=1-2 keV in the observer's frame) by galaxies whose individual soft X-ray flux is less than s_{max}. The median unresolved SXB is represented by the *black solid horizontal lines*, and its 68% confidence levels by the the *gray region*, bounded by *black dashed lines* (taken from Hickox & Markevitch 2007a),. The *red solid lines* show S_X as a function of various model parameters. Our fiducial model assumes $\Gamma = 2.0$, $s_{max} = 2.4 \times 10^{-18}$ erg s^{-1} cm^{-2}, $\psi_{min} = 0.01 M_\odot$ yr^{-1}, and $z_{max} = 10$. The *upper left panel* shows that ψ_{min} only weakly affects S_X, because the faint end of the star formation function (especially at low z) is not steep. The *upper right panel* shows that S_X depends weakly on Γ, provided that $\Gamma \lesssim 2$. The *lower left panel* shows that S_x also depends weakly on s_{max}, unless $s_{max} \lesssim 10^{-18}$ erg s^{-1} cm^{-2}. The *dotted vertical line* shows the X-ray detection threshold in CDF-N (Alexander et al. 2003). The *black filled circle* on this *line* shows the unresolved SXB derived by Hickox & Markevitch (2006, i.e. before subtracting the contribution from X-Ray faint HST detected sources). The *gray region* here brackets the effective minimum X-ray flux s_{min} that is probed by stacking X-ray undetected HST sources (see § 2.1). The *lower right panel* shows that S_X again depends weakly on z_{max}, provided that $z_{max} > 4$. See the main text for a more detailed interpretation of these plots. These plots show that *star forming galaxies that are too faint to be detected as individual X-ray sources, can account for the full unresolved SXB*, and that this statement is insensitive to details in the model when $\Gamma \lesssim 2$, which is reasonable given the available observational constraints (Swartz et al. 2004).

assumed a lognormal conditional probability functions for $P(\log L_X | L_Y)$, where L_Y denotes the galaxy luminosity in some other band Y.

4.2 Results

Our fiducial model assumes $\Gamma = 2.0$ (which corresponds to Γ_{pk}, see above), $s_{max} = 2.4 \times 10^{-18}$ erg s^{-1} cm^{-2} (close to the middle of the range for s_{min} that was quoted in § 2.1) , $\psi_{min} = 10^{-3} M_\odot$ yr^{-1}, and $z_{max} = 10$. As mentioned previously, we explore two choices for extrapolating the star formation rate function with redshift, which likely bracket the range of physically plausible models. When we evolve $\psi^*(z)$, but keep Φ^* fixed, we find that our fiducial model gives $S_X = 2.4 \times 10^{-13}$ erg s^{-1} deg^{-2} cm^{-2}. On the other hand, when we evolve $\Phi^*(z)$, but keep ψ^* fixed, we obtain $S_X = 2.6 \times 10^{-13}$ erg s^{-1} deg^{-2} cm^{-2}. The fact that this difference is small is encouraging, and suggests that our ignorance of the star formation rate function at $z > 0$ does

not introduce major uncertainties into our calculations. We have verified that the second model generally yields slightly higher values for S_X. To be conservative, we focus on the first model in the reminder of this paper.

Figure 2 has four panels, each of which shows the median unresolved soft X-ray background (*black solid lines*), and its 68% confidence levels (the *gray region*, bounded by *black dashed lines*) from Hickox & Markevich (2007b). The *red solid bands* show the contribution from galaxies whose individual soft X-ray flux (1-2 keV observed frame) is less than s_{max}.

• In the *upper left panel* we plot S_X as a function of ψ_{min}. We find that S_X depends only weakly on ψ_{min}. That is, very faint galaxies do not contribute significantly to S_X. This is because the majority of the contribution to S_X comes from galaxies at $z < 2$ (see below, and Fig. 1), where the 'faint' end of the star formation function increases as $\propto \psi^{-1.5}$, and the overall star formation rate density is domi-

nated by galaxies that are forming stars at a rate close to ψ^*.

• The *upper right panel* shows S_X as a function of Γ. We find that S_X decreases with Γ. As most of the contribution to S_X comes from galaxies at $z < 2$, we are most sensitive to the X-ray emissivity of star forming galaxies at $E = [1-2] \times (1+z) < [3-6]$ keV (restframe). For fixed L_X, increasing Γ reduces the fraction of the emitted flux at these 'higher' energies for steeper spectra (i.e. most of the energy lies near $E = 0.5$ keV for the steepest spectra), which results in a decrease in S_X.

• The *lower left panel* shows S_X as a function of $s_{\max}$. The *vertical dotted line* shows the detection threshold in the *Chandra Deep Field-North* (Alexander et al. 2003; Hickox & Markevitch 2007a). The *gray region* here brackets the effective minimum X-ray flux $s_{\min}$ that is probed by stacking X-ray undetected HST sources (see § 2.1). Clearly, S_x depends only weakly on $s_{\max}$, unless $s_{\max} \lesssim 10^{-18}$ erg s^{-1} cm^{-2}. This weak dependence on $s_{\max}$ at larger fluxes can be easily understood: most of the contribution to S_X comes from $z \lesssim 2$ (see below). For galaxies at $z = 1$, $s_{\max} = 2.4 \times 10^{-18}$ erg s^{-1} cm^2 corresponds to $L_X = 4\pi d_L^2(z) s_{\max} / \mathcal{L}_X(z,\Gamma) = 2.9 \times 10^{40}$ erg s^{-1}, which requires $\psi = 9.7 M_\odot$ yr^{-1}, which is close to ψ^*. We are therefore practically integrating over the full UV-luminosity function. Boosting $s_{\max}$ therefore barely increases S_X further.

• The *lower right panel* shows S_X as a function of $z_{\max}$. This plots shows that S_X evolves most up to $z_{\max} \sim 2$, and barely when $z_{\max} \gtrsim 4$. That is, galaxies at higher redshift barely contribute to S_X as we also showed in Figure 1 (unless the conversion factor c_X between L_X and SFR changes with redshift, see § 5).

The main point of Figure 2 is that it shows that *star forming galaxies that are too faint to be detected as individual X-ray sources, can account for the full unresolved SXB*, and that this statement is insensitive to details in the model when $\Gamma \lesssim 2$ over the energy range 1-6 keV. This last requirement is very reasonable, given that the mean observed $\langle \Gamma \rangle = 1.7$ for the majority of ULXs (Swartz et al. 2004).

5 CONSTRAINING THE REDSHIFT EVOLUTION OF THE SFR-L_X RELATION

5.1 Constraints from the SXB

Since our fiducial model already saturates the unresolved SXB, we can ask what constraints we can set on the redshift-dependence of the L_X-SFR relation[3]. Clearly, the SXB can only put constraints on models in which c_X increases with

---

[3] As we already stated in § 1, there are several additional candidate sources which contribute to the unresolved SXB (see § 6 for a summary). To constrain the evolution of c_X we will conservatively allow the entire unresolved SXB to be produced by HMXBs (and the hot ISM) in X-ray faint star-forming galaxies. Obviously, this results in upper limits on possible evolution in c_X.
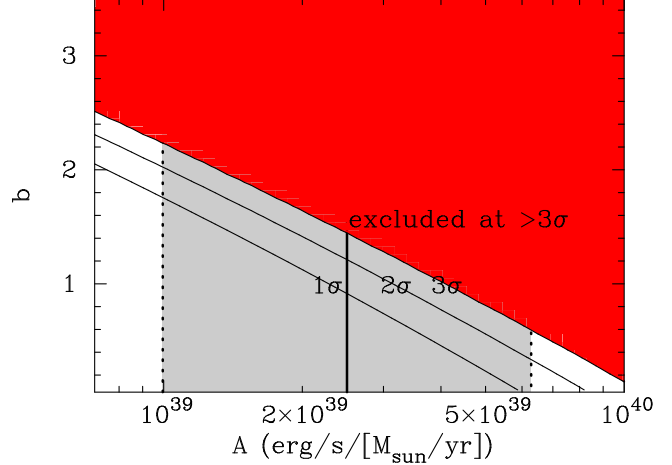

Figure 3. The unresolved SXB constraints on the parameters A and b for a redshift evolution parametrization of the form $c_X \equiv \frac{L_X}{\text{SFR}} = A(1+z)^b$. Models that lie in the *red region* saturate the unresolved SXB at $> 3\sigma$ (see § 5.1). The *grey region* denotes the value for $c_X(z = 0) \equiv A$ derived by Mineo et al. (2011b) (the *solid vertical line* denotes their best-fit value). For this value of A, $b \lesssim 1.3$ (at 2σ).

redshift. We consider models for which

$$\frac{L_X}{\text{SFR}} = c_X \equiv A(1+z)^b, \tag{6}$$

with $b \geqslant 0$, and investigate the constraints that the SXB places on the parameters A and b. We compute S_X (see Eq. 3) on a grid of models which cover a range of A and b. Figure 3 shows how many $\sigma (= 1.4 \times 10^{-13}$ erg s^{-1} cm^{-2} deg^{-2}) above the median observed unresolved SXB, $S_{\text{obs}} = 3.4 \times 10^{-13}$ erg s^{-1} cm^{-2} deg^{-2}, the models lie. Models that lie above the uppermost *solid line*, indicated by the label '3-σ' result in $S_X - S_{\text{obs}} > 3\sigma$. That is, these models significantly overproduce the unresolved SXB and are practically ruled out. The *light grey region* bounded by the *dotted vertical lines* indicates the 68% confidence region for the observed value for c_X by Mineo et al. (2011b), where we assumed 0.4 dex uncertainty on c_X. Their best-fit value for c_X is indicated by the *solid vertical line*. Figure 3 shows that for this value of A, $b \lesssim 1.6$ at $\gtrsim 3\sigma$. If we marginalize[4] over A, then we also get $b \lesssim 1.6$.

We also investigate changes in the SFR-L_X relation of the form

$$c_X \rightarrow f \times c_X \begin{cases} \text{model I} & \text{SFR} \leqslant x \ M_\odot \ \text{yr}^{-1}; \\ \text{model II} & \text{SFR} \geqslant y \ M_\odot \ \text{yr}^{-1} \\ \text{models III\&IV} & z \geqslant z_c \end{cases} \tag{7}$$

The *upper left panel* of Figure 4 shows S_X as a function of f for model I for $x = 0.1$ (*red band*) and $x = 0.5$ (*green band*). This plot shows that $f \gtrsim 3-5$ for $x = 0.1$ is at odds with the

---

[4] We obtain this marginalized upper limit $\mathcal{U}(b) = \int_{A_{\min}}^{A_{\max}} dA \ \mathcal{U}(b|A) P_{\text{prior}}(A)$. Here, $\mathcal{U}(b|A)$ denotes the upper limit on b given A, and $P_{\text{prior}}(A)$ denotes our prior on the probability density function for A. Since $A \equiv c_X(z = 0)$, we took $P_{\text{prior}}(A)$ to be a lognormal distribution with $\langle \log c_X \rangle = 39.4$, and $\sigma = 0.4$ (Mineo et al. 2011b). Finally, we adopted $A_{\min} = 10^{38.5}$ erg s$^{-1}[M_\odot$ yr$^{-1}]^{-1}$, and $A_{\max} = 10^{40.5}$ erg s$^{-1}[M_\odot$ yr$^{-1}]^{-1}$.
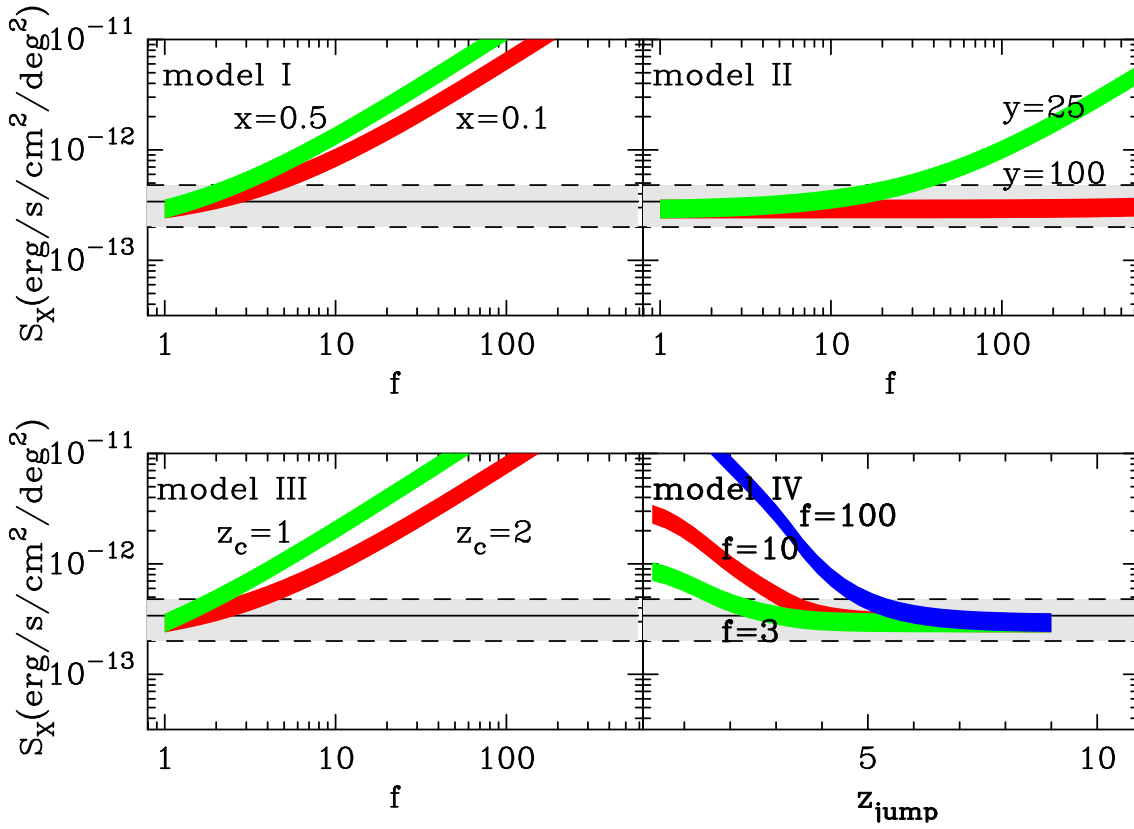
Figure 4. Same as Figure 2, but we modify our fiducial model such that the X-ray emission from star forming galaxies is boosted by a factor of $c_X \rightarrow f \times c_X$ (i.e. $L_X \rightarrow f \times L_X$) when SFR$< x \ M_\odot \ \mathrm{yr}^{-1}$ (*top left panel*), SFR$> y \ M_\odot \ \mathrm{yr}^{-1}$ (*top right panel*), and z$> z_\mathrm{c}$ (*lower left panel*) as a function of f. The *lower right panel* shows a model where we boost c_X by a factor of 100 (*upper blue band*), 10 (*middle red band*) and 3 (*lower green band*) at redshift z_jump as a function of z_jump. This figure shows that even small boosts (i.e. $f \sim$ a few) for SFR$< 0.1 M_\odot \ \mathrm{yr}^{-1}$ or $z \geqslant 2$ violates the constraints posed by the unresolved SXB. It also shows that boosting c_X at the large SFR end barely affects S_X. While large 'jumps' in c_X are not allowed if these occur at low redshift (i.e. $z \lesssim 3$), the unresolved SXB cannot constrain large jumps at $z > 5$.

unresolved SXB. This can be understood from the *top left panel* of Figure 2, which shows that adopting $\psi_\mathrm{min} = 0.1 M_\odot$ yr^{-1} results in $S_X \sim 1.9 \times 10^{-13}$ erg s^{-1} cm^{-2} deg^{-2}, which corresponds to a reduction of $\sim 25\%$. Hence, galaxies with $0.001 < \frac{\mathrm{SFR}}{M_\odot \ \mathrm{yr}^{-1}} < 0.1$ contribute $\sim 25\%$ to S_X (for $f = 1$). Boosting their contribution by a factor $f \gtrsim 3 - 5$ (the exact number depends on the precise fiducial choice for c_X) causes S_X to exceed the unresolved SXB.

The *upper right panel* shows that the soft XRB only allows constraints to be put on $f \gtrsim 10$, and only if $y \lesssim 25$. Strong constraints on f are not possible for large ψ. This is because galaxies that are forming stars at a rate $\psi \gtrsim 100 M_\odot$ yr^{-1} are deep in the exponential tail of the star formation function. As a result of their small number density, they barely contribute anything to S_X.

The *lower left panel* shows that boosting c_X at $z \geqslant 2$ by factors greater than $f \gtrsim 3 - 5$ is again at odds with the unresolved SXB. This is because galaxies at $z > 2$ contribute noticeably to S_X for our fiducial choice of c_X. However, the unresolved SXB cannot place tight limits (yet) on c_X at very high redshifts. This is illustrated in the *lower right panel* where we show S_x for model IV: once $z_\mathrm{jump} \gtrsim 5$, boosting c_X by as much as ~ 100 has little impact on S_X.

5.2 Constraints from the Galaxy XLFs?

As part of our analysis, we compute theoretical galaxy X-Ray luminosity functions (XLFs) using equation (3). Observed galaxy XLFs have been presented, for example, by Norman et al. (2004); Georgantopoulos et al. (2005); Georgakakis et al. (2006); Tzanavaris & Georgantopoulos (2008). Tzanavaris & Georgantopoulos (2008) present galaxy XLF for late-type (i.e. star forming) galaxies in two redshifts bins: the first bin contains galaxies with $0 < z < 0.4$ ($z_\mathrm{med} = 0.14$), and the second bin contains galaxies with $0.4 \leqslant z < 1.4$ ($z_\mathrm{med} = 0.68$). Note that Tzanavaris & Georgantopoulos (2008) derive X-Ray luminosities in the 0.5-2.0 keV band, and we properly K-correct our models into their band.

In Figure 5 the *data points* show the observed X-Ray luminosity functions (XLFs) from Tzanavaris & Georgantopoulos (2008), while the *red dotted line* shows the best-fit Schechter function derived by Georgakakis et al (2006). The *solid lines* show predictions for our fiducial model $c_X = A(1+z)^b$ with $A = 2.6 \times 10^{39}$ erg s^{-1} $[M_\odot \ \mathrm{yr}^{-1}]^{-1}$, and $b = 0.0$. At $z \leqslant 0.4$ our model provides a good fit at the two brightest X-ray luminosities, but overpredicts the number density of fainter sources by a factor of $\sim 2 - 3$. We obtain a better fit if we lower $A = 1.4 \times 10^{39}$ erg s^{-1}/$[M_\odot \mathrm{yr}^{-1}]$,

which corresponds to ~ 0.2 dex, and thus lies within the dispersion that was found by Mineo et al. (2011b). This lower value of A corresponds to almost exactly the value quoted by Lehmer et al (2010, their β, although these authors measured L_X in the 2.0-10.0 keV range). At higher redshift, our model significantly underpredicts the number density at $L_{X,0.5-2.0} \gtrsim 10^{41}$ erg s^{-1}. This may suggest that either that the XLFs (strongly) favor c_X to increase towards higher redshift, and/or SFR $\gtrsim$ a few tens of $M_\odot$ yr^{-1} (see below). Alternatively, the observed XLFs of star forming galaxies are contaminated by low luminosity AGN, which are difficult to identify at these X-ray luminosities.

Our predicted XLFs agree quite well with previous predictions by Ranalli et al. (2005), for the model in which they assume that the redshift evolution of the luminosity functions is solely the result of evolution in the number density of galaxies (this is referred to as 'density evolution'). Their model also underpredicts the number density of luminous X-ray sources at higher redshift. Ranalli et al. (2005) found that a better fit to the high-redshift data is obtained for a model in which solely the luminosity of galaxies evolves ('luminosity evolution') as $\propto (1+z)^{2.7-3.4}$. Our work also indicates that evolution in the number density of star forming galaxies is not enough to explain the observed redshift evolution of XLFs, and that some additional luminosity evolution is preferred.

It is possible to compute the likelihood $\mathcal{L}(A,b) = \exp[-0.5\chi^2]$ by fitting to the observed XLFs for any combination of A and b describing the redshift evolution of c_X (see Eq. 6). However, we found that this formal fit is dominated by the two lowest luminosity data points at $z \leqslant 0.4$, which lie significantly below the XLF that was derived by Georgakakis et al. (2006). Furthermore, we found that this procedure also depends somewhat on the assumed redshift evolution of the star formation rate function. We therefore do not pursue a detailed statistical analysis on constraining the redshift evolution of c_X with the XLFs. Instead, we show in Figure 6 *an example* of a model where c_X increases both with redshift and at high SFR: this model with $A = 1.4 \times 10^{39}$ erg s^{-1} $[M_\odot$ yr$^{-1}]^{-1}$, $b = 1.0$, and $c_X \to 3c_X$ at SFR$\geqslant 15 M_\odot$ yr^{-1} fits the observed XLFs much better. The value $b = 1.0$ is consistent with the X-ray background constraint (see Fig. 3), and boosting c_X by a factor of 3 at SFR$\geqslant 15 M_\odot$ yr^{-1} is also consistent with the soft XRB (see the *top right panel* of Fig. 4). However, boosting c_X by a factor of 3 at SFR$\geqslant 15 M_\odot$ yr^{-1} appears inconsistent with direct constraints on the L_X-SFR relation. In Figure 6 we used $c_X = 4.2(1 + z) \times 10^{39}$ erg s^{-1} $[M_\odot$ yr$^{-1}]^{-1}$ at SFR $\gtrsim 15 M_\odot$ yr^{-1} which translates to $c_X = 8.4 \times 10^{39}$ erg s^{-1} $[M_\odot$ yr$^{-1}]^{-1}$ at $z = 1$, while Mineo et al. (2011b) found $c_X = 3.7 \times 10^{39}$ erg s^{-1} $[M_\odot$ yr$^{-1}]^{-1}$ for their sample of unresolved, high SFR, sources at $z \sim 0.2 - 1.2$. However, the sample of high-SFR, high-z galaxies that was studied by Mineo et al. (2011b) is rather limited, and if the dispersion around this mean quantity is also 0.4 dex, then our model may be consistent with the observed dispersion around this value out to $z \sim 1$.
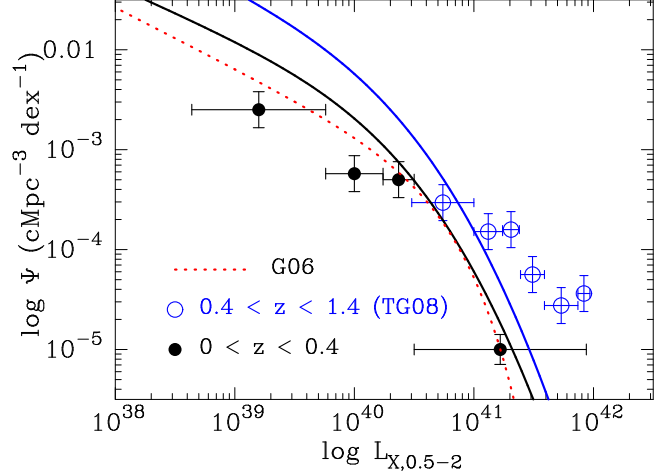

Figure 5. The observed X-Ray luminosity functions (XLFs) of galaxies from Tzanavaris & Georgantopoulos (2008, *data points*) and Georgakakis et al (2006, the *red dotted line* shows their best-fit Schechter function) are compared to our fiducial model $c_X = A(1+z)^b$ with $A = 2.6 \times 10^{39}$ erg s^{-1} $[M_\odot$ yr$^{-1}]^{-1}$, and $b = 0.0$. At $z \leqslant 0.4$ our model provides a good fit at the two brightest X-ray luminosities, but overpredicts the number density of fainter sources by a factor of $\sim 2 - 3$. The $z \leqslant 0.4$ XLF prefers c_X to be lower by ~ 0.2 dex, within the dispersion found by Mineo et al. (2011b). At higher redshift, our model significantly underpredicts the number density at $L_{X,0.5-2.0} \gtrsim 10^{41}$ erg s^{-1}. This suggests that either $b > 0$, or that c_X increases at high ψ (see text).
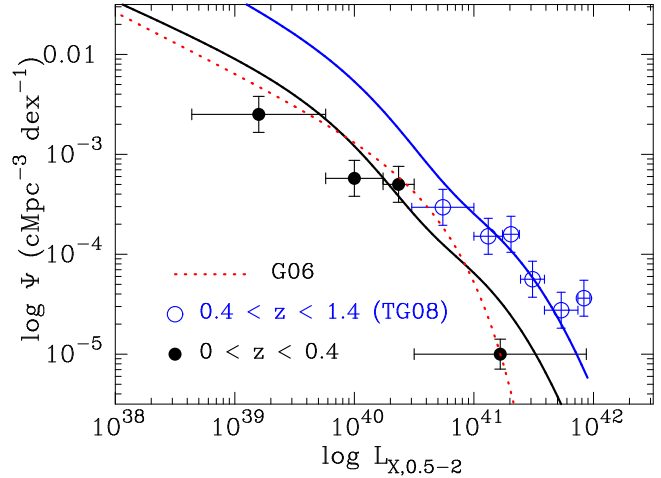

Figure 6. Same as Figure 5, except that here we improved the fit to the observations by forcing c_X to evolve with redshift and star formation rate. The model now assumes $c_X = A(1+z)^b$ with $A = 1.4 \times 10^{39}$ erg s^{-1} $[M_\odot$ yr$^{-1}]^{-1}$, and $b = 1.0$. Furthermore, we boosted c_X by a factor of ~ 3 at SFR $\gtrsim 15 M_\odot$ yr^{-1}. This plot illustrates that the XLFs favor an increase of c_X with redshift and/or at larger SFR.

6 DISCUSSION & CONCLUSIONS

Observations have established that a correlation exists between the star formation rate of galaxies and their X-ray luminosity (measured over the range E=0.5-8 keV, e.g. Ranalli et al. 2003, Grimm et al. 2003, Gilfanov et al. 2004, Lehmer et al. 2010, Mineo et al. 2010). This 'L_X-SFR relation' encodes a wealth of information on various astrophysical pro-

cesses, and strongly affects the thermal evolution of the intergalactic medium during the early stages of the epoch of reionization. Existing observations have only been able to probe this relation in nearby galaxies, and while theoretically there are good reasons to suspect that $c_{\rm x} \equiv L_{\rm X}/{\rm SFR}$ increases towards higher redshifts, observational constraints are virtually non-existent.

In this paper, we have investigated whether it is possible to put any constraints on the evolution of $c_{\rm x}$ with either redshift and/or towards high/low star formation rates than probed by existing observations of individual galaxies. As part of our analysis, we have computed that the observed 'local' relation, when combined with the most observational constraints on the redshift-evolution of the star formation rate density of our Universe, implies that star forming galaxies contribute $\sim 5 - 15\%$ of both the soft and $\sim 1 - 20\%$ of the hard X-ray backgrounds (see § 3). The ranges that we quoted are for a range of photon index $1 < \Gamma < 3$. The observed Γ of ULX spectra in the Chandra bands is described by a distribution with a mean of $\langle \Gamma \rangle = 1.7$, and a mode of $\Gamma_{\rm pk} \sim 2.0$ (Swartz et al. 2004). For the range $\Gamma = 1.7 - 2.0$ the fractional contribution of star forming galaxies to the soft X-ray background is $\sim 8 - 13\%$. The contribution to the HXB remains uncertain, mostly because of a more uncertain K-correction at the corresponding high energies (also see Treyer & Lahav 1996; Natarajan & Almaini 2000, for earlier calculations of the contribution of star forming galaxies to the CXBs).

We have then taken the most recent observational constraints on the star formation rate function, which gives the comoving number density of star forming galaxies as a function of their star formation rate [denoted by $n(\psi, z)$], and computed what the contribution of 'X-ray faint' star forming galaxies to the soft X-ray background (SXB, corresponding to 1-2 keV in the observed frame) is. We found that galaxies whose individual observed flux is $s \leqslant s_{\rm max} = 2.4 \times 10^{-18}$ erg s^{-1} cm^{-2} between 1-2 keV, i.e. more than an order of magnitude fainter than the detection threshold in the *Chandra Deep Field-North* (see § 2.1), can fully account for the unresolved SXB. This statement is insensitive to details in the model as longs as the photon index, averaged over the entire population of X-ray emitting star forming galaxies, is $\Gamma \lesssim 2$, which corresponds to a very reasonable range given the existing observational constraints on this parameter (§ 4).

Motivated by our result that X-ray faint star forming galaxies can fully account for the unresolved SXB, we put constraints on the redshift evolution of the parameter $c_{\rm X}$. When we parametrize the redshift evolution as $c_{\rm X} = A(1+z)^b$, we found that the unresolved SXB requires that $b \lesssim 1.6$ (3σ). We have also ruled out models in which $c_{\rm X}$ is boosted by a factor of $f \gtrsim 2 - 5$ at $z \geqslant 1 - 2$ and/or SFR $\leqslant 0.1 - 0.5 M_\odot$ yr^{-1}, as they overproduce the unresolved SXB (see *left panels* of Fig. 4). We have found indications in the observed X-ray luminosity functions (XLFs) of star forming galaxies that $c_{\rm X}$ is increasing towards higher redshifts and/or higher star formation rates , but caution that this may indicate the presence of unidentified low luminosity AGN. The unresolved SXB allows for larger changes in $c_{\rm X}$ at large values for SFR (see the *top right panel* of Fig. 4). Finally, we also found that the SXB puts weak constraints

on possible strong evolution $(f \sim 100)$ at $z > 5$ (see the *lower right panel* of Fig. 4)[5].

There are many other undetected candidate sources which likely also contribute to the unresolved SXB. These are briefly summarized below (see Dijkstra et al. 2004, for a more detailed summary):

• Observed AGN account for $\sim 80\%$ of the SXB. It would be highly unlikely that fainter AGN– i.e. those are too faint to be detected as individual X-ray sources–do not provide a significant contribution to the unresolved SXB.

• Our attention has focused on HMXBs, but low mass X-Ray binaries (LMXBs)-in which the primary has a mass $\lesssim 5 M_\odot$, dominate the X-ray luminosity of galaxies for which the specific star formation is sSFR $\lesssim 10^{-10}$ yr^{-1} (Gilfanov et al. 2004; Lehmer et al. 2010). LMXBs give rise to a correlation between X-ray luminosity and total stellar mass, M_*, which is $L_{\rm X,LMXB} \sim 9 \times 10^{28} M_*$ erg s^{-1} (Gilfanov 2004; Lehmer et al. 2010). In Appendix C we repeat the calculation of § 4 and replace the star formation rate function $n(\psi, z)$ with the stellar mass function $n(M_*, z)$, and appropriately replace $P(\log L_{\rm X} | \psi)$ with $P(\log L_{\rm X} | M_*)$. We found that faint 'quiescent' galaxies contribute about an order of magnitude less to the SXB than faint star-forming galaxies.

• Thomson scattering of X-rays emitted predominantly by high-redshift sources can cause 1.0-1.7% of the SXB to be in a truly diffuse form (Sołtan 2003). Similarly, intergalactic dust could scatter X-rays by small angles into diffuse halos that are too faint to be detected individually (Petric et al. 2006; Dijkstra & Loeb 2009).

• Wu & Xue (2001) computed that clusters and groups of galaxies possibly contribute as much as $\sim 10\%$ of the total SXB.

• A (hypothetical) population of 'miniquasars' powered by intermediate mass black holes may have contributed to ionizing and heating the IGM (Madau et al. 2004; Ricotti & Ostriker 2004). These miniquasars would emit hard X-ray photons that could contribute significantly to the soft and hard X-ray backgrounds (Ricotti & Ostriker 2004; Dijkstra et al. 2004).

The likely existence of these additional contributors to the unresolved SXB implies that our constraints are conservative, and that actual limits on the redshift evolution of $c_{\rm X}$ should be tighter.

After our paper was submitted, Cowie et al. (2011) compared the average X-ray fluxes (obtained by a stacking analysis) and restframe UV flux densities of sources with known redshifts in the 4 Ms exposure of the CDF-S field. Cowie et al. (2011) showed that this ratio –after an extinction

---

[5] Treister et al. (2011) stacked 197 HST detected candidate $z \sim 6$ galaxies and found significant X-ray detections in both the soft (0.5-2.0 keV) and hard (2.0-8.0 keV) bands (but see Cowie et al. 2011 and Willott 2011). They derive an average rest frame 2-10 keV luminosity of $L_{\rm X,2-10} = 6.8 \times 10^{42}$ erg s^{-1}, which they associate with obscured AGN. We can use this detection to place an upper limit on $c_{\rm X}$ at $z = 6$. The mean star formation rate –averaged over the UV-luminosity function in the range $-21.5 < M_{\rm UV} < -18.0$, and not corrected for dust– is $\sim 2 M_\odot$ yr^{-1}. The stacked X-ray detection therefore puts an upper limit on the boost $f \leqslant L_{\rm X,2-10}/1.5 c_{\rm X} \sim 10^3$. We verified that such a boost at $z_{\rm jump} \leqslant 6.2$ is ruled out at 95% CL.

correction– was consistent with the local L_X–SFR relation up to $z \sim 4$. The stacking of many source allowed Cowie et al. (2011) to probe down to $s \sim s_{max}/4 = 5 \times 10^{-19}$ erg s^{-1} cm^{-2}, which translates to a luminosity of $L_X \sim 0.3-4\times10^{40}$ erg s^{-1} at $z = 1-3$. Cowie et al. (2011) therefore probe the redshift-evolution of c_X at SFR $\gtrsim 1 - 10 M_\odot$ yr^{-1} at these redshifts (depending on z and c_X). For comparison, we have shown that the SXB allows for constraints at lower SFR, but that the SXB becomes less sensitive to changes in c_X at $z \gtrsim 2$. Our results in combination with those of Cowie et al. (2011) thus provide stronger constraints on the allowed redshift evolution of c_X. Interestingly, a non-evolution in c_X with redshift appears at odds with the observed redshift evolution in the XLFs (unless these are contaminated by low luminosity AGN, see above).

Constraints on the redshift evolution of the L_X–SFR relation will be helpful in pinning down the astrophysics that is driving the L_X-SFR relation, and may eventually give us new insights into the X-ray emissivity of the first galaxies which plays a crucial role in determining the thermal history IGM during the dark ages (Mirabel et al. 2011).

REFERENCES

Alexander, D. M., et al. 2003, AJ, 126, 539

Alvarez, M. A., Pen, U.-L., & Chang, T.-C. 2010, ApJL, 723, L17

Arnouts, S., et al. 2005, ApJL, 619, L43

Belczynski, K., Kalogera, V., & Bulik, T. 2002, ApJ, 572, 407

Bogdan, A., & Gilfanov, M. 2011, arXiv:1106.3435

Bothwell, M. S., et al. 2011, arXiv:1104.0929

Bouwens, R. J., Illingworth, G. D., Blakeslee, J. P., & Franx, M. 2006, ApJ, 653, 53

Bouwens, R. J., Illingworth, G. D., Franx, M., & Ford, H. 2007, ApJ, 670, 928

Bouwens, R. J., Illingworth, G. D., Franx, M., & Ford, H. 2008, ApJ, 686, 230

Bouwens, R. J., et al. 2009, ApJ, 705, 936

Cole, S., et al. 2001, MNRAS, 326, 255

Cowie, L. L., Barger, A. J., & Hasinger, G. 2011, arXiv:1110.3326

Dijkstra, M., Haiman, Z., & Loeb, A. 2004, ApJ, 613, 646

Dijkstra, M., & Loeb, A. 2009, MNRAS, 397, 1976

Dray, L. M. 2006, MNRAS, 370, 2079

Furlanetto, S. R., Oh, S. P., & Briggs, F. H. 2006, Phys. Rep., 433, 181

Georgakakis, A. E., Chavushyan, V., Plionis, M., Georgantopoulos, I., Koulouridis, E., Leonidaki, I., & Mercado, A. 2006, MNRAS, 367, 1017

Georgantopoulos, I., Georgakakis, A., & Koulouridis, E. 2005, MNRAS, 360, 782

Gilfanov, M. 2004, MNRAS, 349, 146

Gilfanov, M., Grimm, H.-J., & Sunyaev, R. 2004, MNRAS, 347, L57

Grimm, H.-J., Gilfanov, M., & Sunyaev, R. 2003, MNRAS, 339, 793

Helfand, D. J., & Moran, E. C. 2001, ApJ, 554, 27

Hickox, R. C., & Markevitch, M. 2006, ApJ, 645, 95

Hickox, R. C., & Markevitch, M. 2007a, ApJ, 671, 1523

Hickox, R. C., & Markevitch, M. 2007b, ApJL, 661, L117

Hogg, D. W., Baldry, I. K., Blanton, M. R., & Eisenstein, D. J. 2002, arXiv:astro-ph/0210394

Hopkins, A. M. 2004, ApJ, 615, 209

Hopkins, A. M., & Beacom, J. F. 2006, ApJ, 651, 142

Kaaret, P., Schmitt, J., & Gorski, M. 2011, arXiv:1108.2426

Kajisawa, M., Ichikawa, T., Tanaka, I., et al. 2009, ApJ, 702, 1393

Komatsu, E., et al. 2009, ApJS, 180, 330

Lehmer, B. D., Alexander, D. M., Bauer, F. E., Brandt, W. N., Goulding, A. D., Jenkins, L. P., Ptak, A., & Roberts, T. P. 2010, ApJ, 724, 559

Linden, T., Kalogera, V., Sepinsky, J. F., Prestwich, A., Zezas, A., & Gallagher, J. S. 2010, ApJ, 725, 1984

Madau, P., Rees, M. J., Volonteri, M., Haardt, F., & Oh, S. P. 2004, ApJ, 604, 484

Marchesini, D., van Dokkum, P. G., Förster Schreiber, N. M., et al. 2009, ApJ, 701, 1765

Martin, D. C., et al. 2005, ApJL, 619, L59

Mineo, S., Gilfanov, M., & Sunyaev, R. 2011a, Astronomische Nachrichten, 332, 349

Mineo, S., Gilfanov, M., & Sunyaev, R. 2011b, arXiv:1105.4610, accepted to MNRAS

Mirabel, I. F., Dijkstra, M., Laurent, P., Loeb, A., & Pritchard, J. R. 2011, A&A, 528, A149

Mortlock, A., Conselice, C. J., Bluck, A. F. L., Bauer, A. E., Grützbauch, R., Buitrago, F., & Ownsworth, J. 2011, MNRAS, 373

Natarajan, P., & Almaini, O. 2000, MNRAS, 318, L21

Norman, C., et al. 2004, ApJ, 607, 721

Oh, S. P. 2001, ApJ, 553, 499

Pérez-González, P. G., Rieke, G. H., Villar, V., et al. 2008, ApJ, 675, 234

Persic, M., Rephaeli, Y., Braito, V., et al. 2004, A&A, 419, 849

Persic, M., & Rephaeli, Y. 2007, A&A, 463, 481

Petric, A., Telis, G. A., Paerels, F., & Helfand, D. J. 2006, ApJ, 651, 41

Pritchard, J. R., & Furlanetto, S. R. 2007, MNRAS, 376, 1680

Pritchard, J. R., & Loeb, A. 2010, PRD, 82, 023006

Ranalli, P., Comastri, A., & Setti, G. 2003, A&A, 399, 39

Ranalli, P., Comastri, A., & Setti, G. 2005, A&A, 440, 23

Reddy, N. A., & Steidel, C. C. 2009, ApJ, 692, 778

Ricotti, M., & Ostriker, J. P. 2004, MNRAS, 352, 547

Salpeter, E. E. 1955, ApJ, 121, 161

Sołtan, A. M. 2003, A&A, 408, 39

Swartz, D. A., Ghosh, K. K., Tennant, A. F., & Wu, K. 2004, ApJS, 154, 519

Symeonidis, M., Georgakakis, A., Seymour, N., et al. 2011, MNRAS, 1382

Thomas, R. M., & Zaroubi, S. 2008, MNRAS, 384, 1080

Trac, H., & Cen, R. 2007, ApJ, 671, 1

Treister, E., Schawinski, K., Volonteri, M., Natarajan, P., & Gawiser, E. 2011, *Nature*, 474, 356

Treyer, M. A., & Lahav, O. 1996, MNRAS, 280, 469

Tzanavaris, P., & Georgantopoulos, I. 2008, A&A, 480, 663
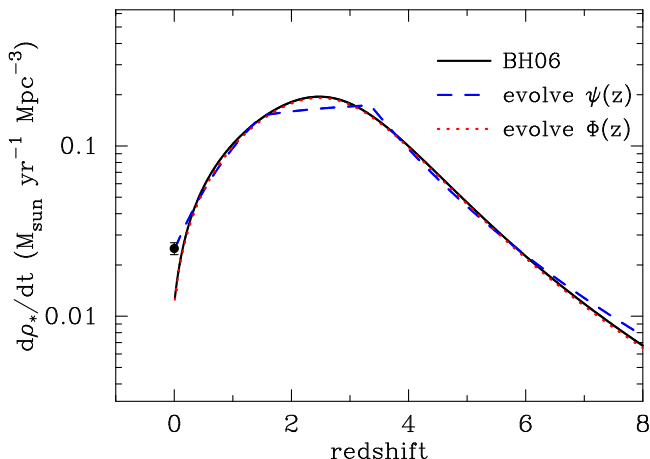
Figure A1. This plot shows the star formation rate density (co-moving) in the Universe, $\dot{\rho}_*(z)$. The *black solid line* shows $\dot{\rho}_*(z)$ that has been derived by Hopkins & Beacom (2006). The data point at $z = 0$ represents the more recent $z = 0$ estimate by Bothwell et al. (2011). The *blue dashed line* (*red dotted line*) shows our model in which we evolve ψ^* (Φ^*) in our adopted star formation rate function with redshift, while keeping Φ^* (ψ^*) fixed. Both models clearly reproduce the 'observed' redshift evolution of the star formation rate density.

Venkatesan, A., Giroux, M. L., & Shull, J. M. 2001, ApJ, 563, 1

Willott, C. J. 2011, arXiv:1110.4118

Wise, J. H., & Cen, R. 2009, ApJ, 693, 984

Wu, X.-P., & Xue, Y.-J. 2001, ApJ, 560, 544

Zheng, Z., Cen, R., Trac, H., & Miralda-Escudé, J. 2010, ApJ, 716, 574

APPENDIX A: ASSUMED REDSHIFT EVOLUTION OF THE STAR FORMATION RATE FUNCTION

A1 The Integrated Star Formation Rate Density

In our paper, we needed to assume the redshift evolution of the star formation rate function $(dn/d\psi)$. We studied two models:

• In our first model, we evolved $\psi^*(z)$ to match the observed star formation rate density, but kept Φ^* fixed. We found that the following redshift evolution of $\psi^*(z)$ provides a decent fit to observations:

$$\frac{\psi^*(z)}{M_\odot \text{ yr}^{-1}} = \begin{cases} 9.2(1+z)^{0.8} & z < z_1; \\ 9.2(1+z_1)^{0.8} & z_1 \leqslant z < z_2 \\ 9.2(1+z_1)^{0.8}\left(\frac{1+z_2}{1+z}\right)^{2.2} & z \geqslant z_2, \end{cases} \quad \text{(A1)}$$

where $z_1 = 1.5$ and $z_2 = 3.35$. The resulting integrated star formation rate density is shown as the *blue dashed line* in Figure A1, which should be compared to that derived by Hopkins & Beacom (2006), which is shown as the *black solid line*. Both curves clearly agree. Note that our adopted star formation rate function–which was compiled from the most recent data–results in a larger star formation rate density at $z = 0$ ($\dot{\rho}_* = 0.025 M_\odot \text{ yr}^{-1} \text{ Mpc}^{-3}$, indicated

by the *black filled circle* at $z = 0$), than that inferred by Hopkins & Beacom (2006), which is $\dot{\rho}_{\text{BH06}}(z = 0) = ah = 0.012 M_\odot \text{ yr}^{-1} \text{ Mpc}^{-3}$.

• In our second model, we evolved $\Phi^*(z)$ to match the observed star formation rate density, but kept ψ^* fixed. We assumed the redshift evolution of $\Phi^*(z)$ was

$$\Phi^*(z) = \Phi^*(z = 0) \times \frac{\dot{\rho}_{\text{HB06}}(z)}{\dot{\rho}_{\text{HB06}}(z = 0)} g(z), \quad \text{(A2)}$$

where the function $g(z) \equiv \frac{1}{2} + \frac{1}{2}(1 + z)^{-1}$ compensates for the fact that the faint-end slope of the star formation rate function, α, changes with redshift in our model. The resulting integrated star formation rate density is shown as the *red dotted line* in Figure A1.

APPENDIX B: DERIVATION OF EQ 1

Eq 1 plays a central role in our analysis. Here, we provide more details on its origin. The total observed flux dS from a proper (i.e physical) cosmological volume element dV_p is $dS(z) = (1 + z)^3 dV_p \dot{\rho}_* \mathcal{L}(z, \Gamma)/4\pi d_L^2(z)$. The cosmological proper volume element dV_p can be written as $dV_p = \frac{c}{H_0} \frac{dz}{(1+z)\mathcal{E}(z)} dA_p$. We substitute $dA_p = d_A^2(z) d\Omega$, where $d_A(z)$ denotes the angular diameter distance to redshift z. We finally get for the differential flux *per sterradian*

$$\frac{dS(z)}{d\Omega} = \frac{c}{H_0} \frac{d_A^2(z)\dot{\rho}_*(z)(1+z)^3 \mathcal{L}(\Gamma, z)}{(1+z)\mathcal{E}(z)4\pi d_L^2(z)} = \frac{c}{4\pi H_0} \frac{\dot{\rho}_*(z)\mathcal{L}(\Gamma, z)dz}{\mathcal{E}(z)(1+z)^2}, \quad \text{(B1)}$$

where we used that $d_A(z) = (1 + z)^{-2} d_L(z)$. When we integrate over redshift and solid angle $\Delta\Omega$, we arrive at Eq 1.

APPENDIX C: CONTRIBUTION OF QUIESCENT GALAXIES TO THE SXB

To compute the contribution of low mass X-ray binaries to the SXB we only need to modify Eq 3 in two ways: (i) we replace the star formation rate function with the observed stellar mass function $n(M_*, z)$, and (ii) we replace $P(\log L_X|\psi)$ with $P(\log L_X|M_*)$. The goal of this appendix is to provide more details of the calculation, and to show that the conclusion that LMXBs contribute about an order of magnitude less to the SXB than HMXBs is robust to uncertainties in the modeling.

Observed stellar mass functions can be described by Schechter functions, and observations have constrained the Schechter parameters out to $z \sim 4$ (e.g. Pérez-González et al. 2008; Marchesini et al. 2009; Kajisawa et al. 2009; Mortlock et al. 2011). In Figure C1 we show results from calculations in which we adopted the parameters from Pérez-González et al. (2008, *red dashed lines*), and Mortlock et al. (2011, *black solid lines*). Both calculations agree well.

We assume that $P(\log L_X|M_*)$ is given by a lognormal distribution, where $\langle L_X \rangle \equiv \mathcal{C}_X M_*$. Here, $\mathcal{C}_X = 8.0 \pm 0.5 \times 10^{28} \text{ erg s}^{-1} M_\odot^{-1}$ (Gilfanov et al. 2004). The scatter in this relation is not given, and for simplicity we have adopted
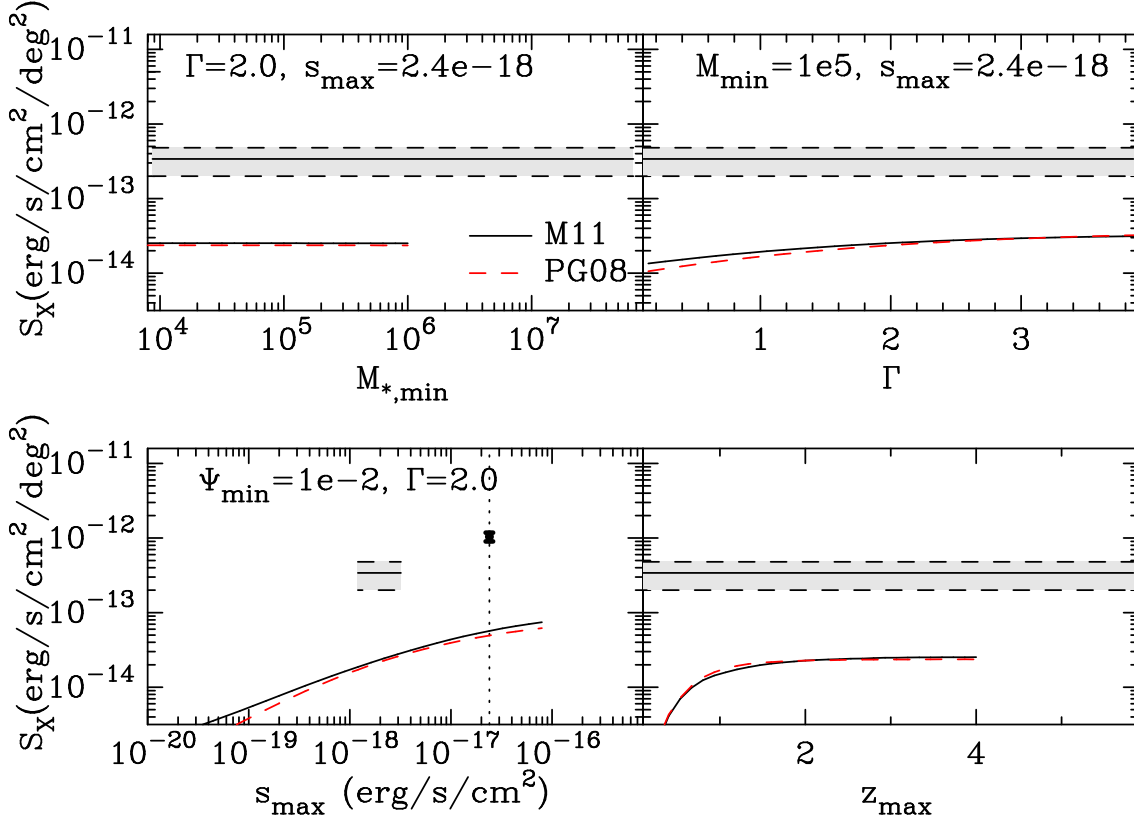
Figure C1. Same as Figure 2, but for low mass X-ray binaries (LMXB), for which the cumulative luminosity scales linearly with the total stellar mass. We integrate the stellar mass functions down to some minimum mass M_{min}. The *upper left panel* shows S_X as a function of M_{min}. Another difference with Figure 2 is that we do not extend our calculation beyond $z_{max} = 4.0$ as the stellar mass functions are constrained poorly at these redshifts. The *black solid lines* [*red dashed lines*] show S_X if we adopt the stellar mass functions from Mortlock et al. (2011) [Pérez-González et al. 2008]. We find that typically, the contribution from LMXBs to the SXB lies about an order of magnitude below that of HMXBs.

$\sigma_1 = 0.4$, but note that our results can simply be rescaled by a factor of $\exp\left(\frac{1}{2}\ln^2 10[\sigma_2^2 - \sigma_1^2]\right)$ to obtain predictions for any σ_2. The last difference with the calculation presented in the main paper is that $L_{X,LMXB}$ is measured in the restframe E$= 2 - 10$ keV band (Lehmer et al. 2010).

Figure C1 presents results from our calculations in a way that is identical to Figure 2 of the main paper. The main differences are: (*i*) the *upper left panel* shows S_X as a function of minimum stellar mass (instead of minimum star formation rate), and (*ii*) our calculations extend only out to $z_{max} = 4.0$, as the observed stellar mass functions become uncertain there. The general trends in this figure are similar to those in Figure 2, except the dependence of S_X on Γ. This different dependence results from the fact that $L_{X,LMXB}$ is measured in the 2-10 keV band (compared to 0.5-8.0 keV for HMXBs) which introduces different K-corrections. Generally, we find that LMXBs produce $S_X \lesssim 3 \times 10^{-14}$ erg s^{-1} cm^{-2} deg^{-2}, which is $\sim 10\%$ of the amount contributed by HMXBs.